

Effective Color Dipole Approach to Color Transparency in ρ^0 Electroproduction

Tae Keun Choi,^{1,*} Kook-Jin Kong,^{2,†} and Byung-Geel Yu^{2,3,‡}

¹*Department of Physics and Engineering Physics, Yonsei University, Wonju 26493, Korea*

²*Research Institute of Basic Science, Korea Aerospace University, Goyang 10540, Korea*

³*Center for Exotic Nuclear Studies, Institute for Basic Science, Daejeon 34126, Korea*

(Dated: July 2, 2026)

We investigate nuclear transparency in exclusive ρ^0 electroproduction on ^{12}C and ^{56}Fe nuclei within a multi-channel final-state interaction (FSI) framework that explicitly incorporates the kinematic decay length effect (DLE) arising from the short-lived $\rho^0 \rightarrow \pi^+\pi^-$ decay. A realistic treatment of the deuteron reference state using the Paris potential wave function, which incorporates the short-range repulsive core and tensor correlations, provides a physically reliable normalization for the transparency ratio T_A/T_D . The conventional DLE and nuclear shadowing mechanisms together remain insufficient to account for the observed Q^2 -dependent enhancement, systematically underestimating the measured transparency throughout the CLAS kinematic range. To address this, we introduce an effective Color Dipole Model (CDM) boundary condition for the initial PLC interaction cross section $\sigma_h(Q^2)$, evaluated as a dipole-weighted average over the $\gamma^*\text{-}\rho^0$ transition wave functions, in place of the purely empirical Quantum Diffusion Model (QDM) ansatz. This CDM-inspired initial condition, combined with the standard linear QDM transport, yields a consistent description of the Q^2 -dependent CLAS data for both targets with an effective in-medium expansion scale $\Delta m^2 = 0.3 \text{ GeV}^2$. Although the present analysis does not provide definitive evidence for the onset of Color Transparency, it demonstrates that a CDM-inspired PLC boundary condition, together with a realistic treatment of the underlying reaction dynamics, yields a physically consistent and quantitatively improved description of the CLAS data.

I. INTRODUCTION

The phenomenon of Color Transparency (CT), a signature prediction of perturbative Quantum Chromodynamics (QCD) in high-energy exclusive nuclear processes, asserts that a hadron can traverse the nuclear medium with reduced attenuation if it is produced in a spatially compact state known as a Point-Like Configuration (PLC) [1, 2]. Because the color dipole moment of a small color-singlet system vanishes with its transverse size, its strong interaction with surrounding nucleons is substantially suppressed—a feature known as color screening [3–5]. Tracking the evolution of this compact system into a fully formed hadron as it propagates through the nucleus provides a unique window into the transition from non-perturbative hadronic degrees of freedom to the fundamental domain of quarks and gluons.

Extensive experimental efforts have sought to establish the onset of CT across various kinematic domains. While clear evidence of CT has been observed in diffractive pion dissociation into di-jets at Fermilab [6] and in exclusive pion electroproduction at Jefferson Lab (JLab) [7, 8], the situation in the baryon sector remains less clear. Recent high-precision data for the $^{12}\text{C}(e, e'p)$ reaction from JLab Hall C showed no indication of CT up to $Q^2 = 14.2 \text{ GeV}^2$ [9], stimulating renewed theoretical discussions regarding the different expansion timescales and configuration dynamics between mesons and baryons.

In the meson sector, exclusive ρ^0 electroproduction on nuclear targets, $A(e, e'\rho^0)A'$, has served as a benchmark for studying CT dynamics. The JLab CLAS collaboration reported a noticeable increase in nuclear transparency with increasing virtuality Q^2 for both ^{12}C and ^{56}Fe targets [10]. However, interpreting these data is complicated by the presence of competing kinematic mechanisms, most notably the Decay Length Effect (DLE) [11, 12]. The DLE arises because the very short lifetime of the ρ^0 meson allows it to decay into a $\pi^+\pi^-$ pair inside the nuclear volume, leading to a momentum-dependent multi-channel absorption. At lower energies, this decay length can be comparable to or smaller than the nuclear radius, leading to a natural variation in the transparency ratio with energy that can mimic the signature of CT.

Several theoretical models have been proposed to analyze the CLAS data. The Kopeliovich-Nemchik-Schmidt (KNS) light-cone dipole approach [13] and the Frankfurt-Miller-Strikman (FMS) semi-classical transport model [11] have attempted to balance the geometric and quantum aspects of the reaction. Nonetheless, drawing a definitive conclusion has been hindered by model-dependent uncertainties, such as the precise modeling of hadronic wave functions and the phenomenological parametrization of the PLC expansion rate.

In this work, we address these challenges by formulating a hybrid theoretical framework that incorporates a Color Dipole Model (CDM) [3, 5] inspired initial boundary condition into a semi-classical multi-channel final-state interaction (FSI) transport description. Within the conventional Quantum Diffusion Model (QDM), a point-like configuration (PLC) is assumed to expand linearly

* tkchoi@yonsei.ac.kr

† kong@kau.ac.kr

‡ bgyu@kau.ac.kr

toward its fully formed hadronic state while propagating through the nuclear medium. However, the initial PLC interaction cross section in the standard QDM is determined through a constituent-quark power-law ansatz rather than from the transverse-size distribution selected at the production vertex. The central novelty of the present approach is not a replacement of the QDM transport picture, but a physically motivated determination of the initial PLC interaction cross section $\sigma_h(Q^2)$ via a dipole-weighted overlap of the γ^* and ρ^0 light-cone wave functions.

The present analysis differs from previous studies in several respects. First, we implement the Paris potential wave function for the deuteron reference state, incorporating the short-range repulsive core and tensor correlations. This provides a realistic treatment of the deuteron structure and a reliable normalization for the transparency ratio T_A/T_D . Second, we explicitly convolve the exponential ρ^0 decay probability with the FSI integrations, so that the DLE is treated as a geometric kinematic effect rather than a correction factor.

Third, we demonstrate that an accurate treatment of the DLE is essential: neglecting the DLE leads to a substantial overestimation of the measured transparency, whereas retaining the DLE and nuclear shadowing alone still fails to reproduce the observed Q^2 dependence. Fourth, we perform a χ^2 comparison against the CLAS data to determine the effective in-medium expansion scale Δm^2 , and we interpret the fitted value $\Delta m^2 = 0.3 \text{ GeV}^2$ as an effective parameter of the semi-classical transport framework rather than a literal identification with a single ρ' excitation mass gap. The framework captures the overall Q^2 dependence and provides a significantly improved description of the CLAS transparency data.

II. THEORETICAL FRAMEWORK

The exclusive electroproduction of ρ^0 mesons on a nuclear target A is induced by a virtual photon γ^* with four-momentum $q = (k - k')$, where k and k' are the four-momenta of the incident and scattered electrons, respectively. The virtuality of the photon is defined as $Q^2 = -q^2$. The nuclear transparency T_A for exclusive ρ^0 electroproduction is defined as the ratio of the nuclear cross section to the free nucleon cross section scaled by the atomic mass number A . Within the semi-classical Glauber framework, it is expressed as an integral over the impact parameter \mathbf{b} and the longitudinal interaction vertex z :

$$T_A = \frac{1}{A} \int d^2\mathbf{b} \int_{-\infty}^{\infty} dz \rho(\mathbf{b}, z) S_{\text{ISI}}(\mathbf{b}, z) S_{\text{FSI}}(\mathbf{b}, z). \quad (1)$$

Here, $\rho(\mathbf{b}, z)$ denotes the nuclear density distribution normalized to A . $S_{\text{FSI}}(\mathbf{b}, z)$ represents the survival probability of the propagating state against final-state inter-

actions (FSI) as it exits the nuclear medium from the production point (\mathbf{b}, z) , and the factor $S_{\text{ISI}}(\mathbf{b}, z)$ accounts for the initial-state interactions (ISI) of the incident virtual photon propagating through the nuclear medium before the hard scattering vertex. S_{ISI} plays a role in incorporating nuclear shadowing effects, and its formulation closely follows the theoretical framework discussed in Ref. [14]. The initial state shadowing is fixed at $\sigma_{\text{ISI}} = 25 \text{ mb}$. This value corresponds approximately to the effective vector-meson-nucleon interaction strength employed in Ref. [14]. To mitigate arbitrary normalization uncertainties, the transparency ratio T_A/T_D is constructed by evaluating the deuteron transparency T_D using the same convolution framework.

A. Nuclear Density Profiles

We utilize a harmonic oscillator (HO) distribution for ^{12}C and a two-parameter Fermi (2pF) profile for ^{56}Fe based on standard electron scattering data. For ^{12}C , the HO density parameters are characterized by a size parameter $a = 1.649 \text{ fm}$ and a fractional parameter $\alpha = 1.247$ [15]. For the heavier ^{56}Fe nucleus, the 2pF profile employs a half-density radius $R = 4.111 \text{ fm}$ and a surface diffuseness parameter $a_0 = 0.558 \text{ fm}$ [16].

For the deuteron ($A = 2$), we employ the Paris potential wave function [17], which incorporates the short-range repulsive core and tensor correlations inherent in the deuteron structure. These features suppress the deuteron density at small internucleon separations, leading to stronger final-state attenuation and consequently a reduced deuteron transparency, T_D . Since the nuclear transparency is extracted as the ratio T_A/T_D , the treatment of the deuteron wave function has a direct quantitative impact on the comparison with experimental data. This sensitivity highlights the importance of a realistic description of the deuteron reference state.

The Paris wave function is evaluated numerically using the parameterization of Ref. [17]. The normalization constant C is determined by numerical quadrature to satisfy $\int |\psi_d(r)|^2 4\pi r^2 dr = 2$, which is verified to better than 0.1%.

B. FSI Convolution and the QDM Expansion

The FSI treats the decay position z_d as an explicit convolution integral over the exponential decay probability:

$$S_{\text{FSI}}(b, z) = \int_z^{\infty} dz_d \left(\frac{1}{l_d} e^{-(z_d - z)/l_d} \right) \times \exp \left[- \int_z^{z_d} \sigma_{\text{eff}}(x, Q^2) \rho(x) dx - \sigma_{\pi\pi} \int_{z_d}^{\infty} \rho(y) dy \right], \quad (2)$$

where x and y denote the longitudinal paths of the ρ^0 and the pion pair, respectively. l_d is the decay length for

$\rho^0 \rightarrow \pi^+\pi^-$. The dynamic decay length in the laboratory frame is formulated as:

$$l_d = \gamma v \tau = \left(\frac{p_\rho}{m_\rho} \right) \left(\frac{\hbar c}{\Gamma_\rho} \right). \quad (3)$$

This exact l_d is computed dynamically for each Q^2 bin, ensuring a precise geometric representation of the decay kinematics. Within the QDM framework, the PLC expands linearly along its formation length $l_f = 2p_\rho \hbar c / \Delta m^2$, where Δm^2 represents the effective expansion scale. The dynamically evolving cross-section is written as:

$$\sigma_{\text{eff}}(z, Q^2) = \sigma_h(Q^2) + (\sigma_{\rho N} - \sigma_h(Q^2)) \frac{z}{l_f}, \quad (z \leq l_f), \quad (4)$$

where the initial effective interaction cross section of the PLC is conventionally estimated from the constituent quark transverse momentum $\langle k_t^2 \rangle^{1/2} \simeq 0.35 \text{ GeV}/c$ [18], yielding

$$\sigma_h(Q^2) = \sigma_{\rho N} \frac{\langle 4k_t^2 \rangle}{Q^2}. \quad (5)$$

The fully expanded ρ - N cross-section is restricted to $\sigma_{\rho N} = 2.5 \text{ fm}^2$ (25 mb), and the uncorrelated pion pair cross-section is set to $\sigma_{\pi\pi} = 5.0 \text{ fm}^2$ (50 mb).

To isolate the role of DLE, additional calculations are performed with the DLE switched off. In this case, the pion-pair interaction is removed by setting $\sigma_{\pi\pi} = 0$, and the decay length is fixed to $l_d = 40 \text{ fm}$. Since this length substantially exceeds the diameter of even the heaviest nuclei considered here ($2R_A \lesssim 20 \text{ fm}$), the produced ρ^0 meson effectively decays outside the nucleus, thereby eliminating pion final-state interactions.

C. Effective CDM Boundary Condition

In the traditional QDM, the cross section expands linearly, but the initial PLC effective interaction cross section σ_h is assigned by the purely empirical constituent-quark power-law ansatz of Eq. (5), which lacks a direct connection to the $q\bar{q}$ size distribution actually selected at the production vertex. To establish a more physically grounded initial condition while preserving the geometric transport structure of the linear expansion, we construct a hybrid framework. Rather than assigning an empirical constant, we determine $\sigma_h(Q^2)$ from the QCD Color Dipole Model (CDM) overlap matrix elements at $z = 0$. The evaluated $\sigma_h(Q^2)$ is then substituted directly into Eq. (4) to govern the FSI expansion. This procedure is motivated by the separation of dynamical scales in the reaction: the production vertex is governed by the transverse-size distribution of the compact $q\bar{q}$ configuration, whereas the subsequent in-medium evolution is adequately described by the established semiclassical QDM transport framework.

The Effective CDM is introduced here only at the level of the initial condition. The QDM linear expansion law and all subsequent FSI integrations are unchanged; only the starting value $\sigma_h(Q^2)$ is replaced by the CDM overlap integral defined below. Within this interpretation, the fitted Δm^2 characterizes the effective in-medium expansion rate of the initially compact ρ^0 configuration rather than a literal single-state excitation mass gap.

The effective PLC interaction cross section $\sigma_h(Q^2)$ is defined as a dipole-weighted average of the dipole cross section over the $\gamma^* \rightarrow \rho^0$ transition overlap:

$$\sigma_h(Q^2) = \int d^2r \int_0^1 dz P_{\gamma^* \rightarrow \rho}(r, z; Q^2) \hat{\sigma}_{\text{dip}}(r, x), \quad (6)$$

where r denotes the transverse separation of the $q\bar{q}$ dipole, z is the light-cone momentum fraction carried by the quark, and x is the effective Bjorken variable entering the dipole cross section, defined as

$$x = \frac{Q^2 + M_\rho^2}{W^2 + Q^2 - m_N^2}, \quad (7)$$

with W the photon-nucleon invariant mass and m_N the nucleon mass. Within the present framework, Eq. (6) should be interpreted as an effective interaction area associated with the compact configurations selected at the production vertex. The transition-overlap weight is defined by

$$P_{\gamma^* \rightarrow \rho}(r, z; Q^2) = \frac{\Psi_\rho^*(r, z) \Psi_{\gamma^*}(r, z; Q^2)}{\int d^2r \int_0^1 dz \Psi_\rho^*(r, z) \Psi_{\gamma^*}(r, z; Q^2)}, \quad (8)$$

which satisfies

$$\int d^2r \int_0^1 dz P_{\gamma^* \rightarrow \rho}(r, z; Q^2) = 1.$$

Accordingly, $P_{\gamma^* \rightarrow \rho}$ acts as a normalized transition-overlap weight selecting the transverse dipole configurations relevant to the $\gamma^* \rightarrow \rho^0$ transition. The overlap weight defined in Eq. (8) is introduced solely as a phenomenological measure of the selected transverse configurations and is not intended to represent a genuine quantum probability density. Consequently, Eq. (6) should be interpreted as an effective interaction measure rather than a strict quantum-mechanical expectation value.

The denominator in Eq. (8) removes the overall transition-overlap normalization and isolates the Q^2 -dependent transverse-size filtering effect. In the small- r region relevant at large Q^2 , the virtual-photon wave function behaves approximately as $\Psi_{\gamma^*} \propto Q K_0(\epsilon r)$, with $\epsilon \sim Q$, so that the overlap is dominated by dipole sizes $r \sim 1/Q$. Since $\hat{\sigma}_{\text{dip}}(r) \propto r^2$ for small dipoles, the numerator contains an additional factor $r^2 \sim Q^{-2}$ relative to the denominator. Parametrically, the denominator

behaves approximately as Q^{-1} , whereas the numerator acquires an additional suppression factor of $r^2 \sim Q^{-2}$ leading to an overall behavior close to $\sigma_h(Q^2) \propto Q^{-2}$. This behavior is well behaved and is consistent with the power-law scaling of the standard QDM ansatz, Eq. (5)

For longitudinal polarization, the light-cone wave function for the virtual photon is given by [19]:

$$\Psi_{\gamma_L^*}(\mathbf{r}, z; Q^2) = \sqrt{N_c} \frac{e \hat{\epsilon}_\rho}{2\pi} \cdot 2z(1-z)Q K_0(\epsilon r), \quad (9)$$

where $N_c = 3$, $\hat{\epsilon}_\rho = 1/\sqrt{2}$, and $\epsilon^2 = z(1-z)Q^2 + m_q^2$ with $m_q = 0.14$ GeV. For the ρ^0 meson, we adopt a simplified Gaussian spatial profile based on the Boosted Gaussian (BG) framework [20, 21]:

$$\Psi_{\rho_L}(\mathbf{r}, z) = N_L z(1-z) \exp\left(-\frac{r^2}{2R_\rho^2}\right), \quad (10)$$

where $R_\rho = 0.73$ fm is chosen as the vacuum electromagnetic radius, and N_L is the normalization constant. By omitting the explicit z -dependent suppression term in the exponential found in standard parameterizations [21], this phenomenological simplification captures the bulk transverse spatial filtering while minimizing excessive model dependencies.

For the dipole-nucleon interaction, we utilize a Golec-Biernat-Wüsthoff (GBW) inspired saturation model [5, 22]:

$$\hat{\sigma}_{\text{dip}}(\mathbf{r}, x) = \sigma_0 \left[1 - \exp\left(-\frac{r^2}{4R_0^2}\right) \right], \quad (11)$$

where the saturation scale R_0 is treated as a constant effective parameter rather than the x -dependent form of the original GBW model. The original GBW parametrization gives

$$R_0(x) = \frac{1}{Q_0} \left(\frac{x}{x_0} \right)^{\lambda/2}, \quad (12)$$

with $Q_0 = 1$ GeV, $x_0 = 3.04 \times 10^{-4}$, and $\lambda = 0.288$. For the CLAS kinematics, $x \simeq 0.1$ – 0.3 , this extrapolation gives $R_0 \simeq 0.45$ – 0.55 fm. Although the small- x dynamics underlying the original GBW fit are not expected to be quantitatively valid in this region, this scale remains physically reasonable for characterizing the onset of color screening in the present intermediate-energy regime: the corresponding crossover scale $r \sim 2R_0$ is of order 1 fm, comparable to a typical hadronic size.

We therefore adopt $R_0 = 0.5$ fm as an effective transverse scale for the GBW-inspired dipole cross section in the present intermediate-energy kinematics. This choice approximately corresponds to the GBW extrapolation evaluated at the mean CLAS kinematics. Since we fix R_0 to a constant value rather than using the x -dependent GBW form, the normalization $\sigma_0 = 2.3$ fm² is adopted as a representative hadronic scale consistent with the original GBW fit [5], without re-optimization.

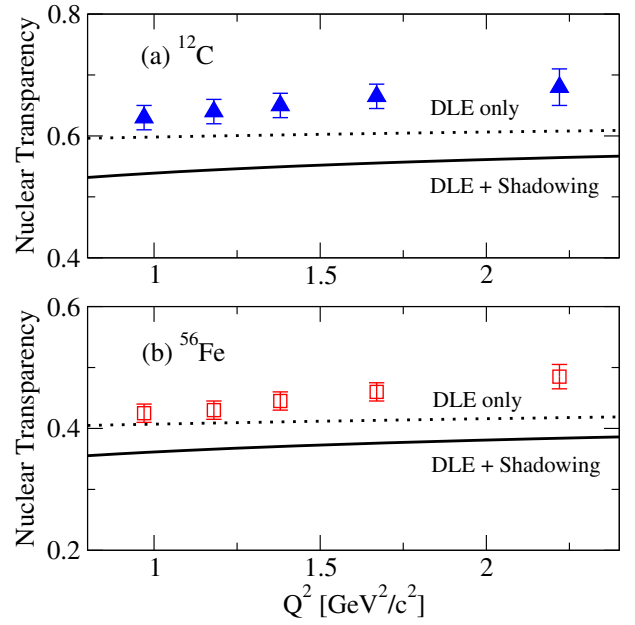


FIG. 1. Nuclear transparency ratio T_A/T_D for ^{12}C and ^{56}Fe . Upward triangles and squares represent data from the JLab CLAS Collaboration [10]. The dotted line represents the Glauber calculation incorporating exclusively the kinematic Decay Length Effect (DLE) with Paris potential wave function [17]. The solid line displays the calculation where both the DLE and standard nuclear shadowing effects are included.

III. RESULTS AND DISCUSSION

All calculations are performed in the laboratory frame using kinematic conditions corresponding to the CLAS experiment of Ref. [10]. The transparency is evaluated using an approximate effective average invariant mass $W = 2.2$ GeV (representing the CLAS experimental range of $W \approx 2.0$ – 2.4 GeV) and momentum transfer in the forward direction ($t \approx t_{\text{min}}$, bounded by $-t \leq 0.4$ GeV²).

In Fig. 1, we examine the capability of purely kinematic and standard nuclear mechanisms to account for the observations. The dotted line displays the transparency obtained when only the kinematic DLE is included, while the solid line additionally includes standard nuclear shadowing effects.

Because the CLAS observable is defined as the ratio T_A/T_D , the extracted transparency depends on the treatment of the deuteron reference state. The realistic Paris wave function therefore provides a reliable normalization for the transparency ratio.

As Q^2 increases, the relativistic decay length l_d increases, reducing the probability of pion absorption inside the nucleus and generating a mild upward trend in both curves. Nevertheless, both calculations remain systematically below the experimental data throughout the measured Q^2 range.

The persistent discrepancy suggests that purely geo-

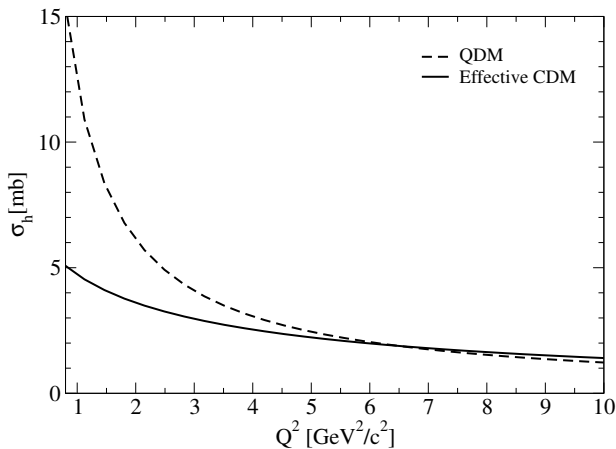


FIG. 2. Effective PLC interaction cross section, $\sigma_h(Q^2)$, as a function of Q^2 . The dashed curve corresponds to the conventional QDM parametrization of Eq. (5), while the solid curve shows the dipole-weighted effective interaction cross section obtained from the Effective CDM overlap integral of Eq. (6). The Effective CDM yields a reduced interaction cross section, particularly at low and intermediate Q^2 , reflecting the preferential selection of compact transverse $q\bar{q}$ configurations in the $\gamma^* \rightarrow \rho^0$ transition.

metric mechanisms, including the DLE and standard nuclear shadowing, are insufficient and that an additional dynamical mechanism associated with the reduced interaction strength of compact PLC configurations is required.

Before presenting the nuclear transparency results, it is instructive to examine the effective PLC interaction cross section itself. Figure 2 shows the Q^2 dependence of $\sigma_h(Q^2)$ obtained from the dipole-weighted overlap integral of Eq. (6), together with the conventional QDM ansatz of Eq. (5). The Effective CDM yields a smaller interaction cross section, particularly in the low- and intermediate- Q^2 region relevant to the present CLAS kinematics. This reduction weakens the initial attenuation of the PLC during its propagation through the nuclear medium, thereby enhancing the survival probability of compact configurations.

Consequently, the Effective CDM predicts a larger nuclear transparency than the standard QDM. This enhancement is a direct manifestation of color screening associated with compact PLC configurations. Furthermore, the Q^2 -dependent decrease of $\sigma_h(Q^2)$ generates the rising Q^2 slope observed in the data. As seen in Fig. 2, the numerical evaluation indeed approaches an approximate Q^{-2} behavior at large Q^2 , consistent with the asymptotic scaling argument derived from Eq. (6). The extended Q^2 range up to 6 GeV^2 is shown to illustrate the asymptotic behavior of $\sigma_h(Q^2)$ and its approximate Q^{-2} scaling at large Q^2 .

To elucidate the role of the CDM boundary condition, Figure 3 displays the calculated transparencies for ^{12}C and ^{56}Fe as a function of Q^2 . The solid lines represent

the Effective CDM results and the dashed lines the standard QDM at the same expansion scale, both evaluated against the CLAS data.

The underlying mechanism is straightforward. The CDM boundary condition $\sigma_h(Q^2)$ evaluated via Eq. (6) is governed by the transverse size of the $q\bar{q}$ configuration selected at the production vertex. As Q^2 increases, the virtual photon wave function $\Psi_{\gamma_L^*} \propto K_0(\epsilon r)$ concentrates weight at smaller transverse separations r . Since $\hat{\sigma}_{\text{dip}} \propto r^2$ at small r , the overlap integral yields a smaller $\sigma_h(Q^2)$ at higher Q^2 , leading to a reduced in-medium attenuation during the early stage of propagation. This Q^2 -dependent modification of the in-medium attenuation distinguishes the CDM boundary condition from the fixed-power QDM ansatz and produces the Q^2 slope observed in the data.

A χ^2 comparison against the ten CLAS data points for both targets simultaneously yields an optimal effective expansion scale $\Delta m^2 = 0.3 \text{ GeV}^2$. The resulting goodness-of-fit for the Effective CDM is $\chi^2 = 1.36$ for ten data points, corresponding to $\chi^2/N_{\text{data}} = 0.14$. Since the model contains a single adjustable parameter, the reduced chi-square becomes $\chi^2/\text{ndf} = 0.15$. For comparison, the standard QDM yields $\chi^2 = 35.06$, corresponding to $\chi^2/N_{\text{data}} = 3.51$ and $\chi^2/\text{ndf} = 3.90$.

The substantially smaller χ^2 obtained with the Effective CDM framework is a direct consequence of the

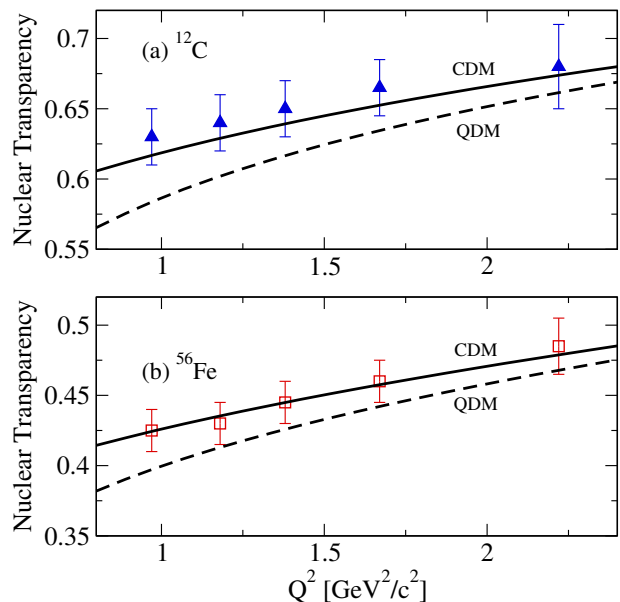


FIG. 3. Nuclear transparency of exclusive ρ^0 electroproduction on ^{12}C and ^{56}Fe as a function of Q^2 within the hybrid effective CDM framework. The solid lines represent predictions obtained with the Effective CDM boundary condition, while the dashed lines correspond to the standard QDM prescription. For the combined data sets, the Effective CDM provides an improved quantitative description of the data compared with the standard QDM.

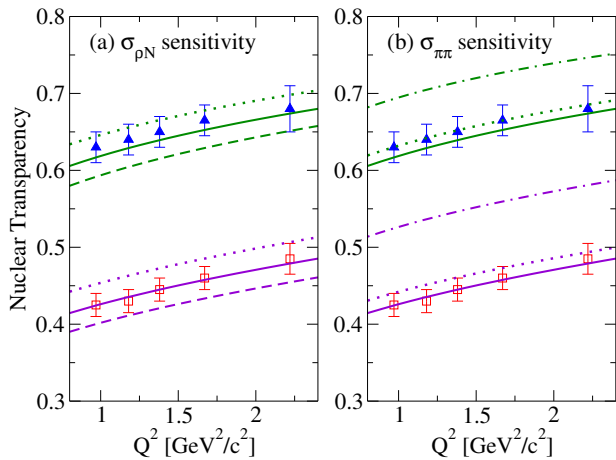


FIG. 4. Sensitivity of the calculated nuclear transparency within the hybrid framework at $\Delta m^2 = 0.3$ GeV². (a) Dependence on the ρN total cross section, with $\sigma_{\rho N} = 20, 25,$ and 30 mb represented by the dotted, solid, and dashed curves, respectively. (b) Dependence on the effective $\pi\pi N$ interaction cross section, where $\sigma_{\pi\pi} = 40$ and 50 mb are shown by the dotted and solid curves, respectively. The data points are the CLAS measurements. The dash-dotted curve shown in the right panel corresponds to the calculation with the DLE deactivated.

of the data. While the conventional QDM captures the overall increasing trend with Q^2 , the Effective CDM reproduces both the magnitude and the Q^2 dependence of the transparency significantly more accurately. This quantitative improvement is achieved without modifying the subsequent QDM transport dynamics, suggesting that the initial PLC boundary condition plays a major role in the description of the present data.

The fitted value $\Delta m^2 = 0.3$ GeV² should be interpreted as an effective in-medium expansion scale within the present semi-classical transport framework rather than as a direct identification with a specific ρ' excitation. The extracted value is smaller than those typically adopted in conventional QDM analyses. However, this difference does not imply a smaller physical excitation mass gap. Because the present framework already incorporates a reduced initial PLC interaction through the CDM boundary condition, the fitted expansion scale effectively absorbs residual medium and transport effects. Consequently, the extracted Δm^2 cannot be directly compared with values obtained in standard QDM implementations.

Figure 4 isolates the effects of varying the effective cross-sections within the nuclear medium, evaluated at the fitted value $\Delta m^2 = 0.3$ GeV². The left panel delineates the dependence on the ρ^0 -nucleon total cross section ($\sigma_{\rho N}$), revealing that the transparency exhibits a noticeable sensitivity to the value of $\sigma_{\rho N}$. Conversely, the right panel evaluates the impact of varying the effective pion absorption cross section ($\sigma_{\pi\pi}$). Variations in $\sigma_{\pi\pi}$ induce only a slight overall shift in the transparency magnitude

without fundamentally altering the shape of the curve. This weak sensitivity arises because the Lorentz boost extends the decay length l_d beyond the nuclear radius at high Q^2 , shifting much of the pion absorption outside the densest nuclear regions. The dash-dotted curve in the right panel, corresponding to the calculation with the DLE deactivated, drastically overestimates the measured transparency at low Q^2 , confirming that an accurate treatment of the decay kinematics is essential for a reliable description of the data.

IV. SUMMARY AND CONCLUSION

We have studied nuclear transparency in exclusive ρ^0 electroproduction within a multi-channel FSI framework that simultaneously treats the kinematic DLE and the dynamical expansion of the initially compact ρ^0 state. The analysis rests on three elements: the Paris potential deuteron wave function as a realistic deuteron reference state, an explicit convolution of the ρ^0 decay probability with the FSI integrations, and a CDM-inspired initial boundary condition for the PLC interaction cross section.

The Paris potential treatment provides a realistic description of the deuteron reference state and establishes a reliable normalization for the transparency ratio T_A/T_D . Standard geometric FSI mechanisms are therefore insufficient: the DLE is necessary to set the low- Q^2 starting point and the correct curvature, but additional color-screening dynamics are required to account for the full Q^2 -dependent enhancement.

The principal finding of this work concerns the role of the initial boundary condition. The standard QDM employs $\sigma_h(Q^2) = \sigma_{\rho N} \langle 4k_i^2 \rangle / Q^2$, an empirical power-law ansatz. Replacing this with the CDM dipole-weighted overlap integral of Eq. (6) introduces a Q^2 -dependent initial interaction area that reflects the transverse size filtering of the production amplitude, while leaving the QDM transport law and all subsequent FSI integrations otherwise unchanged. With this modification, the framework provides an improved description for the Q^2 -dependent CLAS transparency for both ¹²C and ⁵⁶Fe with an effective expansion scale $\Delta m^2 = 0.3$ GeV². This scale should be interpreted as an effective in-medium expansion parameter within the present semi-classical framework rather than a literal ρ' excitation mass gap. The present results do not constitute a definitive proof of Color Transparency; rather, they indicate that a CDM-inspired boundary condition, combined with an accurate treatment of the reaction kinematics, provides a physically consistent and quantitatively improved description of the available data. The present results suggest that the initial PLC boundary condition may play a more important role in CT extractions than previously recognized. Future higher-statistics measurements over an extended Q^2 range will be needed to more stringently test the onset of CT in the vector-meson sector.

ACKNOWLEDGMENTS

This work was supported by the National Research Foundation of Korea (NRF) under Grant No. NRF-2022R1A2B5B01002307 and by the Institute for Basic Science (IBS-R031-D1).

DATA AVAILABILITY

The data supporting the findings of this study are available within the article and from the references cited therein.

-
- [1] A. H. Mueller, in *Proceedings of the Seventeenth Rencontre de Moriond*, edited by J. Tran Thanh Van (Editions Frontieres, Gif-sur-Yvette, France, 1982), Vol. I, p. 13.
- [2] S. J. Brodsky, in *Proceedings of the Thirteenth International Symposium on Multiparticle Dynamics*, edited by W. Kittel, W. Metzger, and A. Stergiou (World Scientific, Singapore, 1982), p. 963.
- [3] N. N. Nikolaev and B. G. Zakharov, *Z. Phys. C* **49**, 607 (1991).
- [4] E. Iancu, K. Itakura, and S. Munier, *Phys. Lett. B* **590**, 199 (2004).
- [5] K. Golec-Biernat and M. Wüsthoff, *Phys. Rev. D* **59**, 014017 (1998).
- [6] E. M. Aitala *et al.* (E791 Collaboration), *Phys. Rev. Lett.* **86**, 4773 (2001).
- [7] B. Clasie *et al.*, *Phys. Rev. Lett.* **99**, 242502 (2007).
- [8] X. Qian *et al.* (Jefferson Lab Hall A Collaboration), *Phys. Rev. C* **81**, 055209 (2010).
- [9] D. Bhetuwal *et al.* (Jefferson Lab Hall C Collaboration), *Phys. Rev. Lett.* **126**, 082301 (2021).
- [10] L. El Fassi *et al.* (CLAS Collaboration), *Phys. Lett. B* **712**, 326 (2012).
- [11] L. Frankfurt, G. A. Miller, and M. Strikman, *Phys. Rev. C* **78**, 015208 (2008).
- [12] K. Gallmeister, M. Kaskulov, and U. Mosel, *Phys. Rev. C* **83**, 015201 (2011).
- [13] B. Z. Kopeliovich, J. Nemchik, A. Schäfer, and A. V. Tarasov, *Phys. Rev. C* **65**, 035201 (2002).
- [14] T. K. Choi, K.-J. Kong, and B.-G. Yu, *Phys. Rev. C* **111**, 064608 (2025).
- [15] C. W. De Jager, H. De Vries, and C. De Vries, *Atomic Data and Nuclear Data Tables* **14**, 479 (1974).
- [16] H. De Vries, C. W. De Jager, and C. De Vries, *Atomic Data and Nuclear Data Tables* **36**, 495 (1987).
- [17] M. Lacombe, B. Loiseau, R. Vinh Mau, J. Côté, P. Pirès, and R. de Tourreil, *Phys. Lett. B* **101**, 139 (1981).
- [18] G. R. Farrar, H. Liu, L. L. Frankfurt, and M. I. Strikman, *Phys. Rev. Lett.* **61**, 686 (1988).
- [19] H. G. Dosch, T. Gousset, G. Kulzinger, and H. J. Pirner, *Phys. Rev. D* **55**, 2602 (1997).
- [20] B. Z. Kopeliovich, J. Nemchik, N. N. Nikolaev, and B. G. Zakharov, *Phys. Lett. B* **324**, 469 (1994); J. Nemchik, N. N. Nikolaev, and B. G. Zakharov, *Phys. Lett. B* **341**, 228 (1994).
- [21] J. Nemchik, N. N. Nikolaev, E. Predazzi, and B. G. Zakharov, *Phys. Lett. B* **374**, 199 (1996).
- [22] K. Golec-Biernat and M. Wüsthoff, *Phys. Rev. D* **60**, 114023 (1999).